Relativistic EOS of Supernova Matter with Hyperons [1]

A. Ohnishi*, C. Ishizuka*, K. Tsubakihara*, H. Maekawa*, H. Matsumiya*, K. Sumiyoshi† and S. Yamada**

*Department of Physics, Faculty of Science Hokkaido University, Sapporo 060-0810, Japan
†Numazu College of Technology, Numazu 410-8501, Japan
**Science and Engineering, Waseda University, Tokyo 169-8555, Japan

Abstract. We investigate hyperon potentials in nuclear matter through hyperon production reactions, and construct several sets of equation of state (EOS) of nuclear matter including hyperons for numerical simulations of core collapse supernovae.

Keywords: supernova, EOS, hyperon, RMF, DWIA
PACS: 26.50.+x, 26.60.+c, 25.80.Hp, 25.80.Nv

INTRODUCTION

The equation of state (EOS) plays an important role in high density phenomena such as neutron stars and supernova explosions. In the core region of neutron stars, the density is so high that hyperons are expected to admix [1, 2]. Especially, the Σ^- baryon has been expected to appear at lower densities than the lightest hyperon, Λ, since it is negative charged and feels a larger chemical potential than neutral and positively charged baryons. Core-collapse processes leading to supernovae or black holes may involve more extreme conditions at high density and temperature. In order to describe the whole evolution of these processes by numerical simulations, one needs to prepare the set of microphysics under such extreme conditions. One of the most important ingredients is the equation of state (EOS) that contains necessary physical quantities. Until now, the two sets of EOS (Lattimer-Swesty EOS [3] and Shen EOS [4]) have been widely used and applied to numerical simulations of core-collapse supernovae. In these EOSs, hyperons are not included, and their applicability is questionable to the long-time evolution such as the proto-neutron star cooling [5] and the black hole formation [6].

In this work, we investigate hyperon potentials in nuclear matter through hyperon production reactions in the distorted wave impulse approximation (DWIA) with a newly developed local optimal Fermi averaging t-matrix (LOFAt) [7, 8, 9]. Next we include hyperons in the nuclear matter EOS with these potential values [10]. We provide the data table covering a wide range of temperature (T), density (ρ_B), and charge-to-baryon number ratio in hadronic part (Y_C), which enables one to apply to supernova simulations.

---

[1] http://nucl.sci.hokudai.ac.jp/~chikako/EOS/

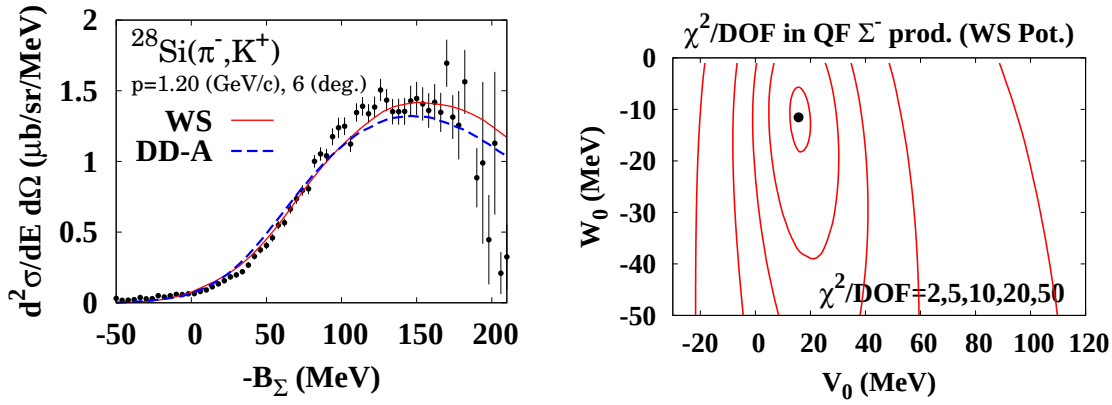

FIGURE 1. Σ^- production spectrum (left) and the χ^2 contour map in the Σ^- production spectrum (right).

HYPERON POTENTIALS IN NUCLEAR MATTER

Hyperon threshold densities and fractions are mainly determined by hyperon potentials in nuclear matter. The Λ-nucleus potential has been known to be around $U_\Lambda = -30$ MeV from single particle energies in the bound state region. It has been naively expected that baryon potential in nuclear matter is proportional to the number of *ud* quarks, suggesting $U_\Sigma \sim U_\Lambda \sim 2/3 U_N \sim -30$ MeV [11], but quark cluster models [12] and a chiral model [13] suggest repulsive potential, $U_\Sigma \sim +30$ MeV. Thus it is very important to determine U_Σ based on real data, not only for astrophysics but also for the understanding of the nature of baryon-baryon interactions.

In extacting Σ and Ξ potentials, presently available data for bound states are so scarce that it is necessary to analyze hyperon production spectra. For Σ, there is only one quasi-bound state ${}^4_\Sigma$He [14], which is too light to extract the potential. For Ξ, no bound state peaks have been specified.

We analyze quasi-free Σ^- production spectra [15] and Ξ^- production spectra [16] in the Green's function method in DWIA [17], in which the hyperon production spectra are represented as,

$$\frac{d^2\sigma}{dE_K d\Omega_K} = \frac{p_K E_K}{(2\pi)^3 v_\pi} R_Y(E_Y)\ , \quad R_Y(E_Y) = -\frac{1}{\pi}\mathrm{Im}\langle i|\hat{\mathscr{O}}^\dagger \hat{t}_q^\dagger \frac{1}{E_Y - \hat{H}_Y + i\varepsilon}\hat{t}_q \hat{\mathscr{O}}|i\rangle\ . \quad (1)$$

Here we show the expression in (π, K^+) reactions as an example, and $\hat{\mathscr{O}}$ denotes the operater which converts πN to $K^+ Y$.

In a standard treatment [17], the elementary t-matrix ($\hat{t}_q$) is assumed to be a constant and factorized out from the response function R_Y, then the cross section is found to be represented as the product of a kinematical factor, the Fermi averaging t-matrix ($\bar{t}_q$) and the strength function, $S = -\mathrm{Im}\langle \hat{\mathscr{O}} \hat{G}_Y \hat{\mathscr{O}}\rangle/\pi$. Recently, it has been pointed out that the on-shell kinematics in the Fermi averaging is important to describe hyperon production spectrum shape [18]. When we have potentials for N and Y, it would be also necessary

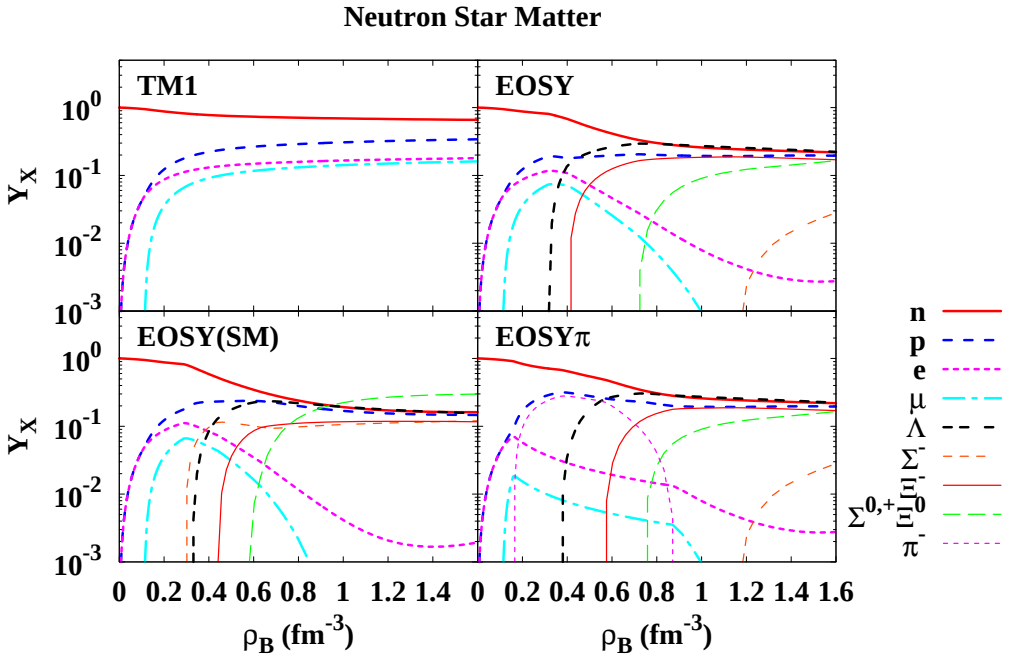

FIGURE 2. Particle number fraction as functions of baryon density in neutron star matter.

to the reaction point dependence [19]. Here we apply the local optimal Fermi averaging t-matrix (LOFAt), $\bar{t}_q(r)$ [7, 8, 9], defined as the Fermi averaging t-matrix under the on-shell condition with hadron single particle local energies containing potential effects.

We show the Σ^- production spectrum in ^{28}Si$(\pi^-, K^+)\Sigma^- X$ in the left panel of Fig. 1, and the χ^2 contour map in the case of Woods-Saxon potential in the right panel of Fig. 1. We find that the Σ^--nucleus potential is well determined to be $U_\Sigma(\rho_0) \simeq (+15\ \mathrm{MeV}, -10\ \mathrm{MeV})$ in the case of the Woods-Saxon potential, which simulates the $t\rho$ approximation. With higher order terms in ρ, $U_Y = \alpha\rho_B + \beta\rho_B^\gamma$, we cannot determine the potential depth only from the quasi-free Σ^- production data, but we find that the spectrum is well described with the potential determined from the Σ^- atomic shift [21]. In the latter case, we need to have more repulsive potential in order to cancel the effects from the attractive potential pocket on the nuclear surface. Thus we may conclude $U_\Sigma > +15$ MeV.

We have also analyzed the Ξ^- production spectra [8], and found that the $U_\Xi \simeq -14$ MeV [16, 20] seems to be reasonable, while we underestimate the absolute value of the production yield for light nuclear target.

EOS WITH HYPERONS AND ASTROPHYSICAL APPLICATIONS

In constructing relativistic EOS with hyperons, we start from the parameter set TM1 [22] and its flavor SU(3) extension [11] for nucleon and hyperon sectors. The RMF parameter set TM1 is determined to describe binding energies and nuclear radii of finite nuclei in

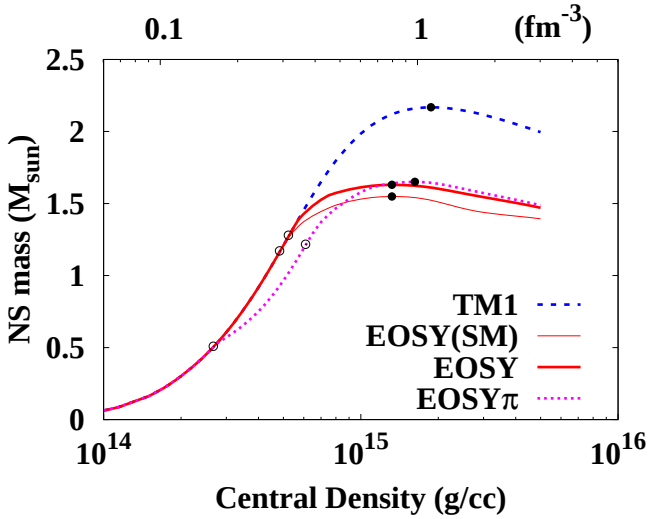

FIGURE 3. Neutron star masses as functions of central density. Filled points show the maximum neutron star masses, and open circles show the threshold densities of hyperons and pions.

a wide mass range. The extension of the RMF to flavor SU(3) has been investigated by many authors. A typical form of the Lagrangian density including hyperons is given as [11],

$$\mathscr{L} = \mathscr{L}_{Free}(B,\sigma,\omega_\mu,\vec{R}_\mu,\zeta,\phi_\mu) - U_\sigma(\sigma) + \frac{1}{4}c_\omega(\omega^\mu\omega_\mu)^2 - \sum_B \bar{\psi}_B\left(g_{\sigma B}\sigma + g_{\omega B}\omega + g_{\rho B}\vec{R}\cdot\vec{t}_B + g_{\zeta B}\zeta - g_{\phi B}\gamma^\mu\phi_\mu\right)\psi_B\ , \tag{2}$$

which contains hidden strangeness ($\bar{s}s$) scalar and vector mesons, ζ and ϕ, in addition to σ, ω and ρ (represented by $\vec{R}^\mu$) mesons.

We adopt the hyperon-vector meson coupling constants based on the SU(6) (flavor-spin) symmetry [11]. Scalar mesons in RMF may partially represent contributions from some other components than $\bar{q}q$, then the hyperon-scalar meson couplings are determined to fit the *recommended* potential strength discussed in the previous section,

$$U_\Sigma^{(N)}(\rho_0) \simeq +30\ \text{MeV}, \quad U_\Xi^{(N)}(\rho_0) \simeq -15\ \text{MeV}\ . \tag{3}$$

Now we apply the EOS with hyperons in the present RMF parameter set (EOSY) to neutron star matter [10]. EOSY is softer than the TM1 EOS due to hyperon admixture at $\rho_B \gtrsim 0.3$ fm^{-3}, as shown in Fig. 2. With attractive hyperon potentials (EOSY(SM)), $(U_\Sigma, U_\Xi) = (-30\ \text{MeV}, -28\ \text{MeV})$ [11], Σ^- appears prior to Λ, and π^- may condensate if the πN repulsion is weak (EOS$Y\pi$). The maximum mass is 1.63 $M_\odot$ for EOSY in contrast to 2.17 $M_\odot$ for nucleonic (TM1) EOS. The central density of a typical neutron star having $1.4M_\odot$ is 0.35 fm^{-3} in nucleonic EOS (TM1), which is a little above the threshold density of Λ in EOSY. In this case, hyperons are limited only in the core region, and the neutron star mass does not get a large reduction as seen in Fig. 3.

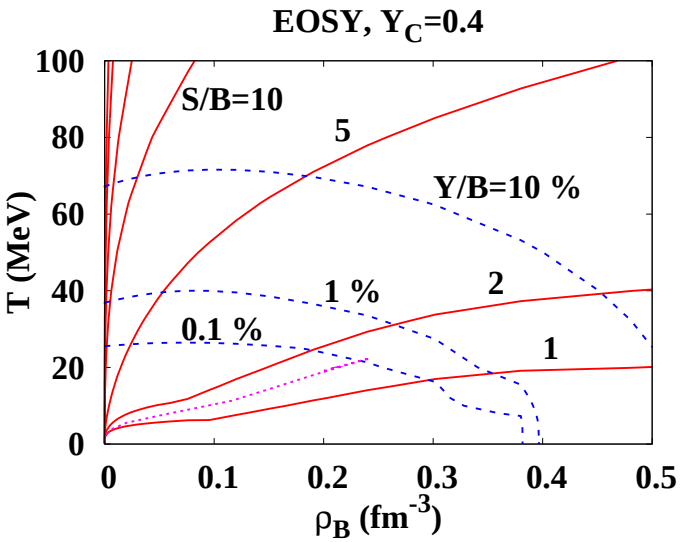

FIGURE 4. Hyperon fraction contours (dashed) and adiabatic paths (solid) in supernova matter at $T = 10$ MeV and $Y_C = 0.4$ in EOSY. The dotted line shows the trajectory of at center during core collapse and bounce.

When we apply the EOS with hyperons to supernova explosions, finite nuclear formation effects are included by adding the differences of the free energy and its derivatives in the Shen EOS and the uniform matter EOS in RMF(TM1) since low density part of EOS is also important. In order to test the EOS table, we calculate the adiabatic collapse of iron core of massive stars with $15M_\odot$ [23] under the spherical symmetry without neutrino-transfer in the same way as Ref. [24]. In Fig. 4, we plot the contour map of the hyperon fraction (sum of strange baryons) in the density-temperature plane. In order to have a significant amount of hyperons, one needs high density or temperature. In supernova core, the entropy per baryon is typically around 1–2 k_B, therefore, one needs high densities 0.3–0.4 fm^{-3} to have 1% mixture of hyperons and 0.45 fm^{-3} for 10%.

We find that in the *model* explosion, caused by the large electron fraction, the maximum density (0.24 fm^{-3}) and temperature (22 MeV) is not high enough for hyperons to appear. However, roles of hyperons must be seen in processes involving higher densties and temperatures or lower electron fractions, such as the thermal evolution of proto-neutron stars [5] and the black hole formation [6].

SUMMARY AND DISCUSSION

In this work, we have investigated hyperon potentials in nuclear matter and extended the Shen EOS by including hyperons with these hyperon potentials.

Hyperon production reactions are analyzed in the distorted wave impulse approximation with a local optimal Fermi averaging t-matrix (LOFAt). We find that the Σ^- and Ξ^- production spectra are well explained with Woods-Saxon potentials. Combined with the Σ^- atom data, we adopt $U_\Sigma = +30$ MeV and $U_\Xi = -15$ MeV as recommended values. These hyperon potentials are included in an SU$_f(3)$ relativistic mean field (RMF) model,

which results in the neutron star maximum mass reduction from $2.17M_{\odot}$ to $1.63M_{\odot}$ with hyperons. We include finite nuclear formation effects at low densities [4], and the supernova matter EOS table is constructed. Hyperon effects are found to be small in prompt supernova explosions, since the matter does not reach the region of hyperon mixture ($Y_Y > 1\%$ for $T > 40$MeV or $\rho_B > 0.4$ fm^{-3}). Hyperon effects should be seen in processes involving higher densties, higher temperatures or lower electron fractions.

ACKNOWLEDGMENTS

This work is supported in part by the Ministry of Education, Science, Sports and Culture, Grant-in-Aid for Scientific Research under the grant numbers, 15540243, 1707005, and 19540252.

REFERENCES

1. N. K. Glendenning, "Compact Stars: Nuclear Physics, Particle Physics and General Relativity" (Springer-Verlag, Berlin, 2000), and references therein.
2. S. Balberg, A. Gal, Nucl. Phys. A **625** (1997), 435.
3. J. M. Lattimer, F. D. Swesty, Nucl. Phys. A **535** (1991), 331.
4. H. Shen, H. Toki, K. Oyamatsu, K. Sumiyoshi, Prog. Theor. Phys. **100** (1998), 1013.
5. H. Suzuki, "Physics and Astrophysics of Neutrinos", edited by M. Fukugita and A. Suzuki (Springer-Verlag, Berlin, 1994), 763; J. A. Pons *et al.*, Astrophys. J. **513** (1999), 780; Astrophys. J. **553** (2001), 382.
6. K. Sumiyoshi, S. Yamada, H. Suzuki, S. Chiba, Phys. Rev. Lett. **97** (2006), 091101; K. Sumiyoshi, S. Yamada, H. Suzuki, Astrophys. J. **667** (2007), 382.
7. H. Maekawa, K. Tsubakihara, A. Ohnishi A 2007 Euro. Phys. J. A **33** (2007), 269.
8. H. Maekawa, K. Tsubakihara, H. Matsumiya, A. Ohnishi, [arXiv:0704.3929 (nucl-th)].
9. H. Maekawa, PhD Thesis, Hokkaido University, March 2008; H. Maekawa, K. Tsubakihara, H. Matsumiya, A. Ohnishi, in preparation.
10. C. Ishizuka, A. Ohnishi, K. Tsubakihara, K. Sumiyoshi, S. Yamada, [arXiv:0802.2318 (nucl-th)]
11. J. Schaffner, I. Mishustin, Phys. Rev. C **53** (1996), 1416.
12. M. Kohno *et al.*, Nucl. Phys. A **674** (2000) 229.
13. N. Kaiser, Phys. Rev. C **71** (2005) 068201.
14. T. Nagae *et al.*, Phys. Rev. Lett. **80** (1998), 1605; T. Harada, S. Shinmura, Y. Akaishi and H. Tanaka, Nucl. Phys. A **507** (1990), 715; T. Harada, Phys. Rev. Lett. **81** (1998), 5287.
15. H. Noumi *et. al.*, Phys. Rev. Lett. **89** (2002) 072301 [Erratum: Phys. Rev. Lett. **90** (2003) 049902]; P. K. Saha *et. al.*, Phys. Rev. C **70** (2004) 044613.
16. T. Fukuda *et al.*, Phys. Rev. C **58** (1998), 1306; P. Khaustov *et al.*, Phys. Rev. C **61** (2000), 054603.
17. O. Morimatsu and K. Yazaki, Nucl. Phys. A **483** (1988) 493; O. Morimatsu and K. Yazaki, Nucl. Phys. A **435** (1985) 727; T. Harada and Y. Akaishi, Prog. Theor. Phys. **96** (1996) 145; M. T. López-Arias, Nucl. Phys. A **582** (1995) 440; S. Tadokoro, H. Kobayashi and Y. Akaishi, Phys. Rev. C **51** (1995) 2656.
18. T. Harada and Y. Hirabayashi, Nucl. Phys. A **744** (2004), 323; Nucl. Phys. A **759** (2006), 143; Nucl. Phys. A **767** (2006), 206
19. M. Kohno *et al.*, Prog. Theor. Phys. **112** (2004) 895.
20. S. Aoki *et al.*, Phys. Lett. B **355** (1995), 45.
21. C. J. Batty, E. Friedman, A. Gal, Phys. Lett. B **335** (1994), 273.
22. Y. Sugahara, H. Toki, Nucl. Phys. A **579** (1994), 557.
23. S. E. Woosley, T. A. Weaver Astrophys. J. Suppl. **101** (1995), 181.
24. K. Sumiyoshi, H. Suzuki, S. Yamada, H. Toki, Nucl. Phys. A **730** (2004), 227.